Nano-structuring of Solid Surface by EUV Ar^{8+} Laser

K. Kolacek[1], V. Prukner[1], J. Schmidt[1], O. Frolov[1], J. Straus[1], A. Shukurov[2], V. Holy[2], J. Sobota[3], T. Fort[3]

[1] Institute of Plasma Physics Academy of Sciences of the Czech Republic, v.v.i., Za Slovankou 1782/3, 182 00 Prague 8, Czech Republic
[2] Faculty of Mathematics and Physics Charles University in Prague, Ke Karlovu 3, 121 16 Prague 2, Czech Republic
[3] Institute of Scientific Instruments Academy of Sciences of the Czech Republic, v.v.i., Kralovopolska 147, 612 64 Brno, Czech Republic

Abstract: The paper demonstrates our first attempt for "direct (i.e. ablation) patterning" of PMMA by pulse, high-current, capillary-discharge-pumped Ar^{8+} ion laser ($\lambda = 46.9$ nm). For focusing a long-focal spherical mirror (R = 2100 mm) covered by 14 double-layer Sc-Si coating was used. The ablated focal spots demonstrate not only that the energy of our laser is sufficient for such experiments, but also that the design of focusing optics must be more sophisticated: severe aberrations have been revealed – an irregular spot shape and strong astigmatism with astigmatic difference as large as 16 mm. In some cases, on the bottom of ablated spots a laser-induced periodic surface structure (LIPSS) has appeared. Finally, an illumination of the sample through quadratic hole 7.5x7.5 μm, standing in contact with PMMA substrate, has ablated from the surface a strongly developed 2D diffraction pattern (period in the centre ~125 nm).

1. Introduction

For a long time micro- and nano-patterning of solid surfaces was motivated by a progress in microelectronics, which, following Moore´s law (doubling every two years the transistor-count that can be placed inexpensively on integrated circuit) [1], commands[1] a continuous upgrade of lithography[2]. Such upgrade indirectly influences processing speed, memory capacity, number and size of pixels in sensors, etc. However, at present the pre-competitive cooperation phase in EUV lithography is over and a few main players solve, how to expose 300-millimeter-diameter wafers with throughput ~100 wafers/hour; in other words, how to ensure on these wafers an energy density 15-20 mJ/(cm^2.shot of EUV radiation), i.e. average EUV power 200 W at the source. This is beyond possibilities of any EUV laser[3]. However, even now, when Moore´s law still holds, there is a notion that some other limit is behind the door [4]: in the mid-2000s microprocessor clock rates stalled near 3 GHz because faster processors generated

[1] Although Moore´s law was initially made in the form of an observation and forecast, the more widely it became accepted, the more it served as a goal for the entire industry. This drove both marketing and engineering departments of semiconducter manufacturers to focus enormous energy aiming at the specified increase so that it would be soon actually attained by one or more competitors. In this regard, it can be viewed as a self-fulfilling prophecy [3].

[2] Here we have in mind a special branch of this technique (called sometimes micro- or nano-lithography) used for fabrication of integrated circuits and micromechanical systems. This lithography comprises many issues: light source (working in EUV/soft X-ray region), debris reduction, projection/illumination optics, mask production/inspection/repair, resist application/exposition/development/etching (not necessary in direct-writing case) etc.

[3] Optical lithography started with visible light source, then shifted to ultraviolet lamps, 248 nm krypton-fluoride lasers, to the present 193 nm argon-fluoride laser. The next technological step was supposed to be the 157 nm molecular-fluorine laser, but problems with the calcium fluoride optics caused hesitation. Instead, developers turned to immersion lithography, which yields a sharper focus of the 193 nm line by directing the light through water. Refinements to immersion lithography allowed fabrication of circuits with a 45 nm half-pitch, and adding a trick called double-patterning shrank the half-pitch down to 32 nm in the last generation of fabrication lines that came on line in 2009. At present the winning new technology for 13.5 nm uses tin droplets of the exactly given size injected in a vacuum chamber; the droplets are hit on their trajectory by a CO_2 laser pulses of exactly given energy (average power 10-20 kW) that evaporate and ionize them.

more waste heat than they could dissipate. Manufacturers got around that performance wall by designing chips with multiple cores, processors that operated in parallel. Yet the new paradigm of multicore processing can't be extended too far without major changes in software and hardware. Software that now performs operations serially must be rewritten to execute operations in parallel on chips with more than 8 or 16 cores [5], and integrated photonics hardware can provide that massive interconectivity. Optics have inherently high bandwidth density, which advanced modulation formats and wavelength-division multiplexing (WDM) can increase to levels far beyond the reach of electronics. Fibre-optic links are already used commercially on backplanes of high-performance computers. The next step is to bring them to the circuit board, where they are expected to be within a couple of years; integration of photonics on electronic chips would follow. Therefore, basic research will continue even in this well developed line and it is worth having a tool for fast nanopatterning that can assist electron beam lithography in production of research-oriented units.

Simultaneously, there are other branches, where low-volume nanofabrication needs periodic nanostructures. One of them is plasmonics (see e.g. [6-8]), which belongs to most rapidly growing areas of physics, with possible applications ranging from sensing and biomedicine to imaging and nanotechnology [9-13], and which amply uses nanoparticles, nanorods, and nanostructures. The nanostructures consisting of multiple metallic elements with controlled relative placements (down to distances of the order of ~10 nm) provides a simple yet compelling way not only to tune the resonance frequencies of the system, but also to change the interaction strength with radiation (due to near-field coupling between neighbouring units)[4]. Among another research items that need nanostructures belong photonic crystals and nanophotonic materials [14, 15], high density magnetic memories [16, 17], miniaturized RF oscillators [18], UV polarizers [19, 20], dense gratings (for determination of ultimate resolution of new photoresists) [21-24]. Currently these nanostructures are fabricated by electron beam lithography and focused ion beam lithography, which is very precise, but simultaneously very slow (point-by-point etching) and expensive. That is why any alternative methods are warmly welcomed.

This paper presents the first step to nanostructure a solid surface by EUV radiation. We used for that a natural-pattern (laser induced periodic surface structure (LIPSS) on the bottom of ablated crater, or 2D diffraction pattern in the windows of in-contact standing grid) created by single imperfectly-focused EUV laser beam.

At the next step a controlled two-beam interaction (interference) pattern will be used, where the fringe spacing could be changed. A design work is in progress.

2. Apparatus

Experiments with nanostructuring of PMMA were performed on our older apparatus CAPEX (see Fig. 1).

The CAPEX device consists of

- Marx generator, 8 stages, erected capacity 12.5 nF, erected voltage 400 kV, stored energy 1 kJ,

[4] The full development of nanoplasmonics was delayed by the lack of devices that can generate coherent plasmonic fields. It was proposed that in the same way as a laser generates stimulated emission of coherent photons, a “spaser” could generate stimulated emission of surface plasmons (oscillations of free electrons in metallic nanostructures) in resonating metallic nanostructures adjacent to a gain medium where absorption loss in metal is compensated (even allows amplification) by optical gain in localized and propagating surface plasmons. Recently such “spaser” was realised [7] with 44-nm-diameter nanoparticles with a gold core and dye-doped silica shell, where losses of localized surface plasmons were fully compensated by gain. Thus surface plasmon resonances were capable of squeezing optical frequency oscillations into a nanoscopic cavity creating a nanolaser with outcoupling of surface plasmon oscillations to photonic modes at a wavelength of 531 nm.

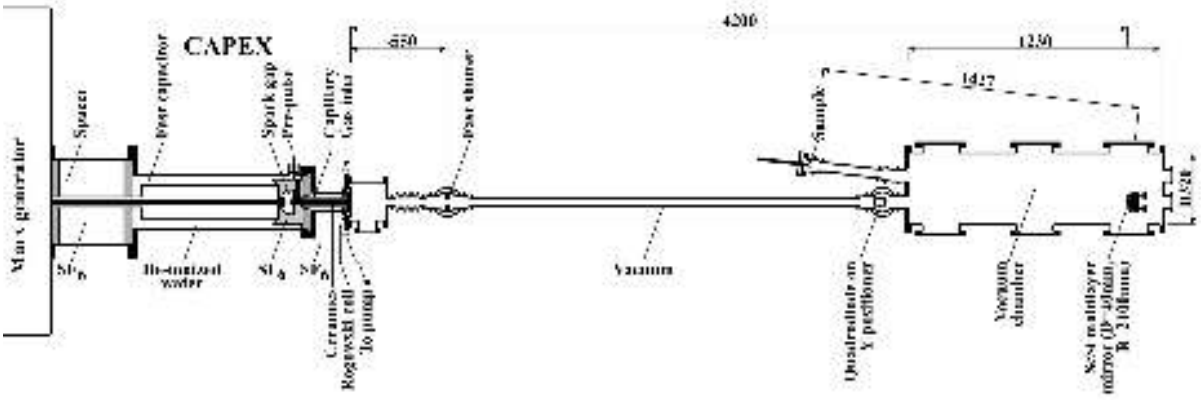

Figure 1. *Apparatus. For nanostructuring experiments the CAPEX device was extended for vacuum tube with fast shutter and quadrodiode, for vacuum chamber with multilayer mirror, and for interaction tube with sample.*

- Spacer, SF_6 filled, which separates oil filled Marx generator and water filled fast capacitor,
- Fast coaxial capacitor, dimensions ∅262x∅158x675, capacitance 6 nF, characteristic impedance 3.37 Ω,
- Spark gap working in a self-breakdown regime,
- Ceramic capillary, dimensions ∅3.2x232, Ar filled,
- Ar filling and pumping assembly, which maintains the optimum Ar pressure in the capillary and sufficient vacuum in the diagnostic and interaction part of the apparatus.

The CAPEX device is capable to deliver the current amplitude of ~50 kA after the current quarter-period ~50 ns.

For nanostructuring experiments the CAPEX apparatus was extended for

- Vacuum tube with
  - ~ Fast mechanical shutter, which allows radiation to pass, but blocks particles and debris ejected from the capillary (due to their longer time-of-flight),
  - ~ Quadrodiode, which enables after two or three shots to find the EUV beam axis and adjust accordingly the vacuum chamber,
- Vacuum chamber with multilayer mirror mechanically controlled from atmospheric side by Double Cardan joints with Wilson vacuum seals,
- Interaction tube with mechanically controlled sample.

3. Multilayer mirror

The design of multilayer mirror was split into two parts. The first one compared focusing properties of spherical mirror with those of off-axis parabola. It turned out that for our configuration (focal length 1050 mm, angle of incident and reflected beams 7.6°) is the diameter of focal spot (where 85% of the beam-energy is concentrated) for spherical configuration ~1.5-times larger than that for the parabolic one, what was considered as acceptable for these measurements (taking also into account higher price and longer production time of the off-axis parabola).

The second part of the design concerned the ScSi multilayer reflecting structure. From available three references for refraction index of Si [25, 26, 30] and four references for index of refraction of Sc [27-30] those published in [30] were used, namely

$$n_{Si} = 0.8074 + i\ 1.82\ 10^{-2},$$
$$n_{Sc} = 0.96703 + i\ 2.85\ 10^{-2}.$$

Reflectivity curves of multilayers were calculated with the modified software developed by prof. Holy (FMP ChU Prague). They indicated that the best are not the layers of equal optical thickness ($n_{Sc}*h_{Sc} = n_{Si}*h_{Si}$, n being Re-part of index of refraction, h being thickness of the layer), but equal geometrical thickness ($h_{Sc} = h_{Si}$) – namely 13 nm with the tolerance +0.2 nm and -0.0 nm. The optimum number of double-layers turned to be 20 (see Fig. 2). After next two iterations that took into account production and technological possibilities our design resulted in layers of equal geometrical thickness (13.15 ± 0.3) nm, and in 14 double-layers with theoretical reflectivity 45% for perpendicular incidence.

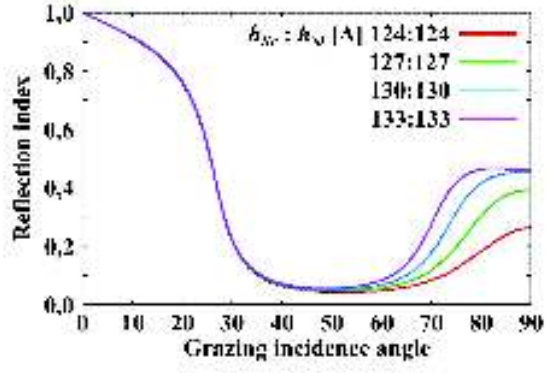

Figure 2. *Reflectivity as a function of grazing incidence angle; parameter of curves is thickness of Sc:Si layers in Å.*

4. Ablation of PMMA by Ar^{8+} laser beam

4.1. Direct exposition and exposition through a large grid

The sample was exposed a few times in different positions and simultaneously photographed by photographic camera. The focused visible light emitted from the capillary was clearly visible on the PMMA surface. These spots on photographs should have assist at identification of position of ablated area. Nevertheless even at this assistance the identification of this position was extremely difficult.

The first ablated spots in PMMA (see Fig. 3) were seen in optical microscope at observation in geometrically reflected light. On the other hand, a similar observation with sample between crossed polarisers did not indicate any residual stress caused by local heating; therefore, it seems confirmed that the ablation is not a result of thermal effects of radiation, but of quantum ones only.

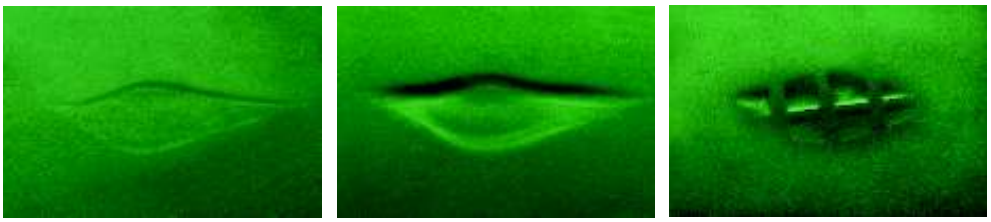

Figure 3. *Left – PMMA ablated by one shot of Ar^{8+} laser. Middle – PMMA ablated by five shots. Right – PMMA ablated through Ni grid (step 100x100 μm, free windows 70x70 μm, traverses 30 μm) by five shots; all these three pictures are in the same scale and with false colours.*

Analysis of these spots by scanning electron microscope was not successful; however, for this analysis the PMMA sample was covered by a thin (transparent) layer of gold. Fortunately,

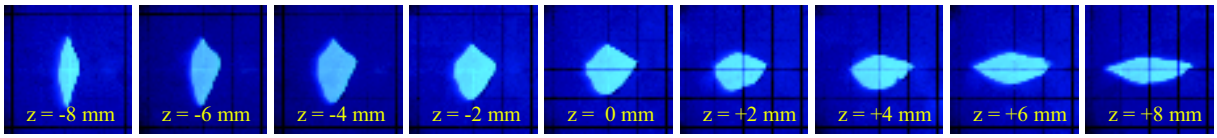

Figure 4. *Z–scan of laser beam footprint on gold-covered PMMA; apparent astigmatism is visible with astigmatic difference ~16 mm; the pictures were taken at blue illumination through microscope the measuring objective of which had grid 125x125 μm/div.*

already the first test shots at this layer showed not only that laser energy is sufficient for ablation of this layer, but also that the laser-beam-footprints are excellently visible even with the naked eye (esp. if the sample is indirectly slightly back-illuminated). In this arrangement we z-scanned the laser-beam-footprint trying to find the best focus (see Fig. 4). Despite focus of the visible light seemed to be at first glance perfect, it turned out that astigmatism of EUV radiation is very strong, astigmatic difference being ~16 mm.

Finally the laser-beam footprint was analysed by atomic force microscope. For this analysis two parts of the spot shown in the middle of the Fig. 3 (ablation by 5 shots, ~8 mm from the central plane, i.e. in the more distant astigmatic focus) were selected: part "A" (150x150 μm) is located in the right corner of the ablated region, while part "B" (150x150 μm) is located in the middle-bottom part of that region. Part "A" as well as part "B" contain both the ablated and the not-ablated regions (see Fig. 5). It is visible that each ablated part has on its surface

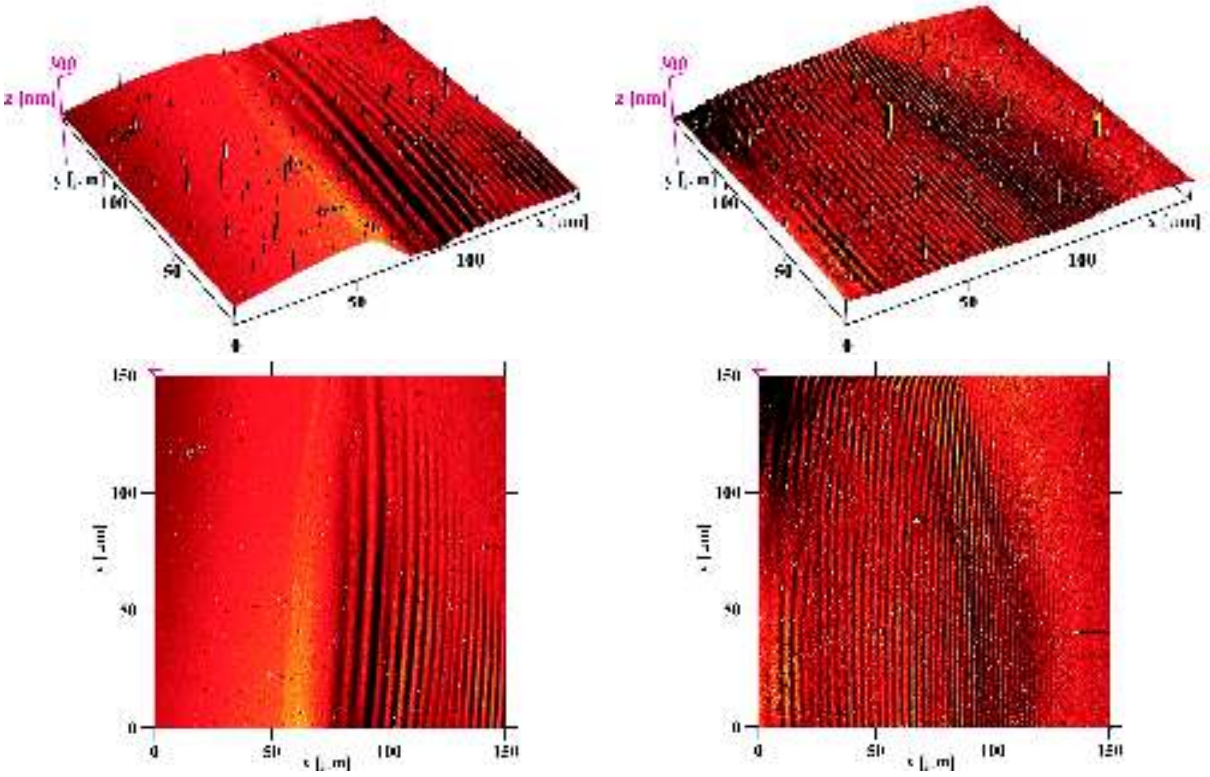

Figure 5. *Spot ablated by five laser shots in the more distant astigmatic focus. Left – region in the right corner. Right – region in the middle-bottom part of the spot. Top – 3D images. Bottom – 2D images.*

more or less contrast periodic structure with period ~2,8 μm and with peak-to-peak depth ~5-10 nm. It offers to attribute these structures to LIPSS (Laser-Induced Periodic Surface Structure) [31-33]. However, on the one side, LIPSS I (LIPSS of the first type) is typically created by a polarised laser light [31] (representing material response to interference of the incidence radiation and the radiation scattered along the surface); contrary, amplified spontaneous emission of our mirror-less laser is not polarised and its reflection from multilayer

mirror at nearly normal incidence practically does not change this fact. On the other side, the mechanism responsible for LIPSS II (LIPSS of the second type) formation is attributed to melting effects [33]: at low fluences, the structure develops when thin molten strips resolidify on the solid substrate, while at high fluences, the structure results from freezing of capillary waves which are generated on the surface that the laser pulse has uniformly melted. Contrary we expect that in our case the quantum ablation plays a dominant role and the thermal effects are negligible. Therefore, despite two types of LIPSS have been already classified, none of them is fully fitting to our case.

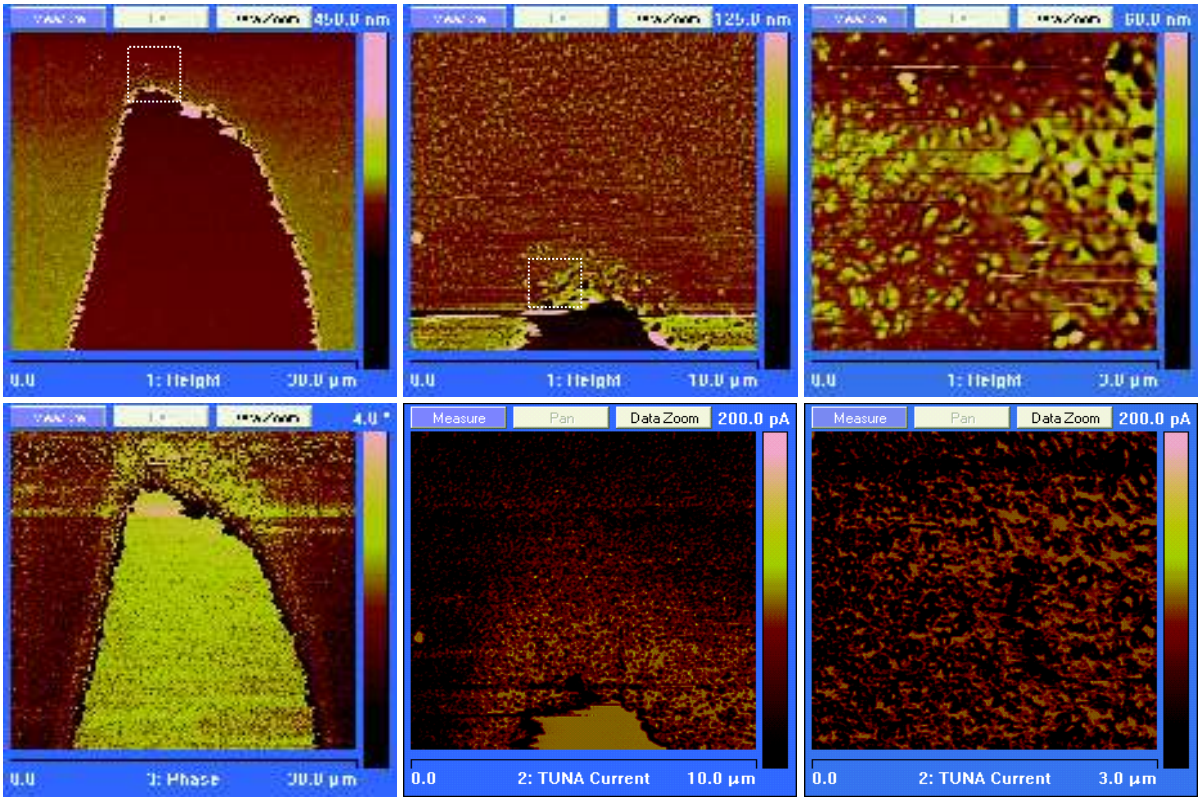

Figure 6. *Analysis of laser-beam footprint on the gold(40 nm)-covered PMMA by AFM. LEFT COLUMN: - upper part of the laser-beam-footprint: upper field – AFM in taping mode indicating height; rectangle defines area shown in the middle column; lower field – taping mode, phase contrast. MIDDLE COLUMN: upper field: taping mode, height; rectangle defines area shown in the right column; lower field: current mode. RIGHT COLUMN: upper field: taping mode, height; lower field: current mode.*

Similarly, ablation of PMMA samples with ~40 nm Au layer have been also analysed by AFM (see Fig. 6). Left column of fields shows the upper part of the laser-beam-footprint. Both fields in this column were taken with AFM in taping mode; the upper field shows height, while the lower one shows phase contrast. Both fields indicate that in this case no periodic surface structure is created. Instead, units-of-micrometers-wide lighter part around the laser-beam-footprint in the lower field is interpreted as PMMA deposited on not-ablated gold layer. The same lighter surrounding around the laser-beam-footprint is visible in an enlarged scale in the middle-bottom-field (taken by AFM in current mode indicating local conductivity). Contrary, in the most enlarged scale (right column of the Fig. 6) no individual particles/grains/solidified-droplets of PMMA on Au were distinguishable (either in the upper field taken by AFM in taping mode measuring height, or in the lower field taken by AFM in current mode measuring local conductivity).

4.2. Exposition through a small grid

Finally, a surface of bare PMMA was irradiated through a small grid (step 12.5x12.5 μm, windows 7.5x7.5 μm) closely attached to this surface (see Fig. 7) with intention to see, if some structure similar to LIPSS is generated even in a limited space like a small grid window.

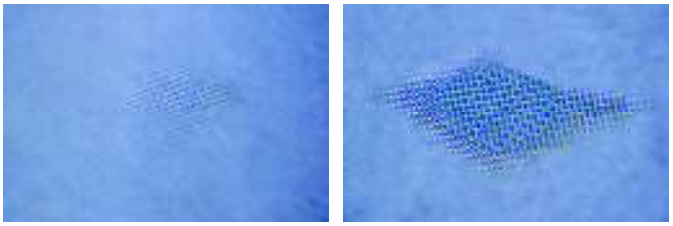

Figure 7. *Bare PMMA ablated through the attached Au grid (step 12.5x12.5 μm, windows 7.5x7.5 μm). Left: ablation by one shot. Right: ablation by five superimposed shots. False colours.*

Also this pattern was analysed by AFM. It turned out that in each grid window a well-developed 2D diffraction pattern was created (see Fig. 8). The period of diffraction pattern changes from ~800 nm (at the edge of window) down to ~125 nm (in the middle of the window). One ridge (possibly a part of LIPSS) can be seen in the mid of the window.

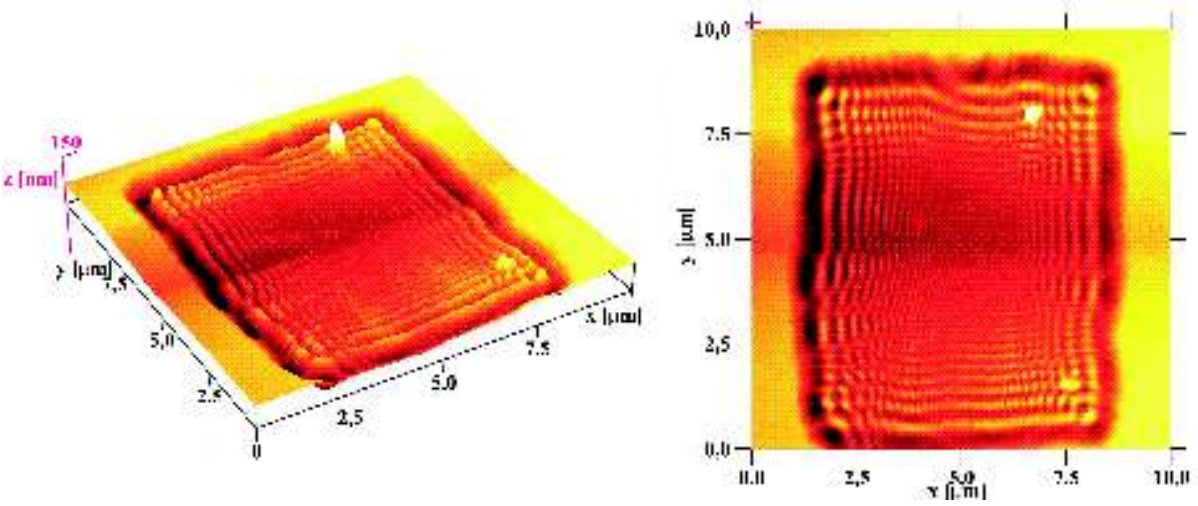

Figure 8. *AFM analysis of the ablated pattern in one grid window (dimension 7.5x7.5 μm). Left: 3D plot. Right: 2D plot.*

Comparison of the ablated pattern with a theoretical profile of diffraction on a rectangular hole (see Fig. 9) confirms that the ablated pattern is really the result of diffraction.

5. Conclusion

It was demonstrated that our EUV Ar^{8+} laser (λ = 46.88 nm), the energy of which has not yet been reliably measured, but is estimated to be tens or hundreds of μJ is capable with focused beam to ablate PMMA, even if the focus is significantly influenced by astigmatismus.
If the beam-footprint on a bare PMMA surface is large, the ablated area is covered by periodic surface structure with periodicity ~2.8 μm. However, it still remains to be proved, whether this pattern can be attributed to LIPSS.

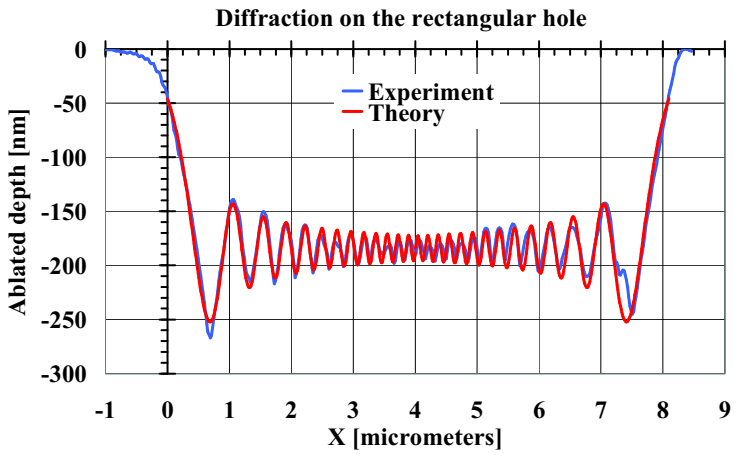

Figure 9. *Diffraction on the rectangular hole 7.5x7.5 μm; horizontal profile 5.3 μm*

If the beam-footprint on a PMMA, covered by a thin (~40 nm) Au-layer, is large, no periodic surface structure has been observed. Instead, around the laser-beam-footprint a few micrometers wide composite area is created, where gold is intermixed with PMMA.
If the beam-footprint on a bare PMMA surface is small and limited by some obstacle, a diffraction pattern is created, the periodicity of which spans down to ~125 nm.
It should be mentioned that there is only a limited possibility to change the periodicity of these surface structures (if they are created). Therefore, a new interferometer is designed, which will be able to create controlled periodic structures with periodicity approaching the laser wavelength (~50 nm in our case).

Acknowledgement

The experimental part of this work was performed under auspices and with the support of the Grant Agency of the Academy of Sciences CR (contract KAN300100702), the theoretical part of this work was supported by the Ministry of Education, Youth, and Sports of the Czech Republic (contracts LA08024 and LC528).

References

[1] MOORE, G.E., "Progress in digital integrated electronics", Electron Devices Meeting (1975) 11-13, where original statement – doubling every year [2] – was corrected
[2] MOORE, G.E., "Cramming more components onto integrated circuits", The experts look ahead, Electronics **38** (1965) 8
[3] DISCO, C., van der MEULEN, B., "Getting New Technologies Together", New York: Walter de Gruyter, ISBN 311015630X, OCLC 39391108, 206-207
[4] HECHT, J., "Photonic integration may boost computing performance", Laser Focus World (March 2011), 57-60
[5] FULLER, S.H., MILLETT, L.I., eds., "The future of computing performance: Game over or next level?", National Research Council (2010); http://bit.ly/eR0e0A
[6] MAIER, S.A., Plasmonics: Fundamentals and Applications, Springer Science + Business Media LLC, New York, 2007
[7] ZOUHDI, S., SIHVOLA, A., Metamaterials and Plasmonics: Fundamentals, Modelling, Applications, Proc. of the NATO Advanced Research Workshop on Metamaterials for Secure Information and Communication Technologies, Marrakech, Morocco, 7-10 May 2008, Springer Science + Business media B.V., Dordrecht (The Netherlands), 2009
[8] KLIMOV, V.V., Nanoplasmonics, Fizmatlit, Moskva, 2009 (in Russian)
[9] NOGINOV, M.A. et al., "Demonstration of spacer-based nanolaser", Nature **460** (August 2009) 1110-1112

[10] SCHULLER, J.A., et al., "Plasmonics for extreme light concentration and manipulation", Nature Materials **9** (February 2010) 193-204
[11] HILL, M.T., "Nanophotonics: Lasers go beyond diffraction limit", Nature Nanotechnology **4** (2009), News and Views, 706-707
[12] WU, W., et al., "Plasmonic enhanced quantum well infrared photodetector with high detectivity", Appl. Phys. Lett. **96** (April 2010), 161107
[13] BAUMBERG, J.J., et al.. "Angle-resolved surface-enhanced Raman scattering on metallic nanostructured plasmonic crystals", Nano Letters **5** (November 2005), 2262-2267
[14] CAMPBELL, M.., et al., "Fabrication of Photonic crystals for the visible spectrum by holographic lithography", Nature **404** (March 2000), 53-56
[15] FAN, W.J., et al., "Large-area, infrared nanophotonic materials fabricated using interferometric lithography", J. Vacuum Science & Technology B **23** (Nov-Dec 2005), 2700-2704
[16] HEYDERMAN, L.J., et al., "Arrays of nanoscale magnetic dots: Fabrication by X-ray interference lithography and characterization", Applied Phys. Letters **85** (Nov 2004), 4989-4991
[17] CHOU, S.Y., KRAUSS, P.R., "65 Gbits/in^2 quantum magnetic disk", J. Appl. Phys. **79** (April 1996), 5066-5066
[18] MANCOFF, F.B., et al., "Phase-locking in double-point-contact spin-transfer devices", Nature **437** (Sep 2005), 393-395
[19] PELLETIER, V., et al., "Aluminum nanowire polarizing grids: Fabrication and analysis", Appl. Phys. Lett. **88** (May 2008), Art. No. 211114
[20] SCING, E.E., et al., "Extreme-ultraviolet polarization and filtering with gold transmission gratings", App. Optics **34** (Feb 1995), 648-654
[21] ANDERSON, C.N., NAULLEAU, P.P., "Do not always blame the photons. Relationship between deprotection blur, line-edge roughness, and shot noise in extreme ultraviolet photoresists", J.Vacuum Science & Technology B **27** (2009), 665-670
[22] NAULLEAU, P.P., et al., "Latest results from the SEMATECH Berkeley extreme ultraviolet microfield exposure tool", J. Vacuum Science & Technology B **27** (2009), 66-70
[23] HOFFNAGLE, J.J., et al., "Use of interferometric lithography to characterize the spatial resolution of a photoresist film", J. Photopolymer Science and Technology **16** (2003), 373-379
[24] HOFFNAGLE, J.J., et al., "Liquid immersion deep-ultraviolet interferometric lithography", J.Vacuum Science & Technology B **17** (1999), 3306-3309
[25] PALIK, E.D., "Handbook of Optical Constants of Solids", 1985, Academic Press
[26] http://physics.nist.gov/PhysRefData/FFast/html/form.html
[27] VINOGRADOV, A.V., "Multilayer X-ray optics", Quantum Electronics **32** (2002) 1113-1121
[28] USPENSII, Y.A., et al., "Efficient method for determination of extreme-ultraviolet optical constants in reactive materials: application to scandium and titanium", J. Opt. Soc. America A – Optics Image Science and Vision **21** (2004) 298-305
[29] FERNANDEZ-PEREA, M., et al., "Determination of optical constants of scandium films in the 20-1000 eV range", J. Opt. Soc. America A – Optics Image Science and Vision **23** (2006) 2880-2887
[30] NIELSEN, J., et al., "Developing multi-layer mirror technology near 45 nm using Sc/Si interfaces", 2004 UCRL-TR-202362
[31] SIPE, J.E., et al., "Laser-induced periodic surface structure. I. Theory", Phys. Rev. B **27** (1983) 1141-1154.
[32] YOUNG, J.F., et al., "Laser-induced periodic surface structure. II. Experiments on Ge, Si, Al, and brass", Phys. Rev. B **27** (1983) 1155-1172.
[33] YOUNG, J.F., et al., "Laser-induced periodic surface structure. III. Fluence regimes, the role of feedback, and details of the induced topography in germanium", Phys. Rev. B **30** (1984) 2001-2015.